Gold–Boron Chemistry. Part 2.[1] The Interaction of $\{AuP(C_6H_{11})_3\}$ Bridges with Decaboranyl Cages: The Accurate Structure of [5,6-μ-$\{AuP(C_6H_{11})_3\}$-*nido*-$B_{10}H_{13}$], and the Synthesis and Molecular and Electronic Structures of its Conjugate Base [5,6,9,10-μ_4-$\{AuP(C_6H_{11})_3\}$-*nido*-$B_{10}H_{12}$]$^-$ †

Andrew J. Wynd and Alan J. Welch *
Department of Chemistry, University of Edinburgh, Edinburgh EH9 3JJ
R. V. Parish
Department of Chemistry, University of Manchester Institute of Science and Technology, P.O. Box 88, Manchester M60 1QD

Analysis of the results of an accurate, low-temperature redetermination of the molecular structure of [5,6-μ-$\{AuP(C_6H_{11})_3\}$-*nido*-$B_{10}H_{13}$] (**1a**) implies an interaction, albeit weak, between the bridging gold atom and the B(9)H(9,10)B(10) moiety, and extended Hückel molecular orbital (EHMO) calculations reveal that the nature of this bonding is interaction of the three-centre two-electron–B(9)HB(10) unit with a previously vacant 6*sp*-hybrid orbital on gold. Mössbauer parameters obtained for (**1a**) are consistent with an *sp*-hybridised gold(I) atom which makes a supplementary weak interaction. Deprotonation of (**1a**) or of its $P(C_6H_4Me\text{-}2)_3$ analogue removes the H(9,10) atom, and affords species (**2**) in which the gold–phosphine unit has slipped from μ to μ_4 on a decaboranyl framework, the molecular structure of $[NHEt_3][nido\text{-}\{AuP(C_6H_{11})_3\}B_{10}H_{12}]$, (**2a**), having been established by a crystallographic study. For (**2**), a combination of Mössbauer spectroscopic studies and EHMO calculations indicates that the orbital number of the metal atom is again somewhat greater than 2, *i.e.* that the formal co-ordination geometry of the gold(I) bridge is intermediate between linear and trigonal, but more so than in (**1**). The deprotonation of (**1**) is fully reversible, and its reaction with HCl results in cleavage of the remaining gold–boron connectivities to afford $B_{10}H_{14}$.

In the first paper in this series[1] we described the synthesis (from $B_{10}H_{14}$) and characterisation of [5,6-μ-$(AuPR_3)$-*nido*-$B_{10}H_{13}$] [R = cyclo-C_6H_{11} (**1a**); C_6H_4Me-2 (**1b**)]. These species are classified as Class 2 gold–boron compounds[1] since the $\{AuPR_3\}$ fragment simply bridges an edge of the decaboranyl cage, isolobally replacing the μ-5,6-H atom of $B_{10}H_{14}$. We are interested in developing the chemistry of compounds (**1**), with particular emphasis on establishing differences between its behaviour and that of $B_{10}H_{14}$ that result from the potentially greater versatility of an $\{AuPR_3\}$ function over hydrogen. In this paper we accordingly describe some of the studies we have completed on compounds (**1**). (*i*) The results of an accurate, low-temperature crystallographic analysis of compound (**1a**) that suggests an interesting Au···B(9)H(9,10)B(10) interaction, and the results of an associated molecular orbital (m.o.) study. (*ii*) Reversible deprotonation of (**1**) that results in non-oxidative slipping of the gold atom, such that in the product (**2**) the B_{10} unit is η^4-co-ordinated; the molecular and electronic structures of (**2a**) have been probed by crystallographic, molecular-orbital, and n.m.r. and Mössbauer spectroscopic studies. (*iii*) Reaction of (**1a**) with HCl that results in cleavage of the gold–boron link and regeneration of $B_{10}H_{14}$.

Experimental

Synthetic and Spectroscopic Studies.—Unless otherwise stated, all reactions were carried out under an atmosphere of nitrogen using Schlenk techniques, with all solvents dried and distilled under nitrogen prior to use. N.m.r. spectra were recorded from CD_2Cl_2 solutions at room temperature on JEOL FX 60 Q (^{31}P), Brucker WP 200 SY (^{31}P, ^1H, ^{11}B) and WH 360 (^1H, ^{11}B) spectrometers, the last fitted with an Aspect 3000 computer. Chemical shifts are relative to external $SiMe_4$ (^1H), 85% H_3PO_4 (^{31}P), and BF_3·OEt_2 (^{11}B), positive values being to high frequency. Techniques for recording ^1H-{^{11}B} spectra have been previously described.[2] Infrared spectra were measured as CH_2Cl_2 solutions on a Perkin-Elmer 598 spectrophotometer. Mössbauer spectra were recorded with source (Au/Pt) and sample immersed in liquid helium, using 256 channels of a Harwell 6000 spectrometer. The spectra were each fitted with two independent Lorentzians, and the isomer shifts are quoted relative to gold foil. Microanalyses were determined by the Departmental service at Edinburgh. Compounds (**1a**) and (**1b**) were prepared as described in ref. 1.

Deprotonation of [5,6-μ-$\{AuP(C_6H_{11})_3\}$-*nido*-$B_{10}H_{13}$], (**1a**). (*With* NEt_3. To a stirred suspension of compound (**1a**) (0.4747 g, 0.794 mmol) in CH_2Cl_2 (20 cm^3) was added, dropwise, NEt_3 (0.080 g, 0.791 mmol) in the same solvent (10 cm^3). The initially colourless solution gradually turned first yellow, then orange, with concomitant dissolution of (**1a**). Finally, all of (**1a**) was consumed and the resultant solution was cherry-red. Removal of solvent *in vacuo* afforded an orange powder, which crystallised from CH_2Cl_2–n-hexane as red *crystals* of the $[NHEt_3]^+$ salt of $[nido\text{-}\{AuP(C_6H_{11})_3\}B_{10}H_{12}]^-$, (**2a**) (0.525 g, 95%) (Found: C, 40.3; H, 8.75; N, 2.00. $C_{24}H_{61}AuB_{10}NP$ requires C, 40.1; H, 9.05; N, 2.05%); $\nu_{max.}$ at 3 100 (N–H), 2 910, 2 840 (both C–H), 2 500 (B–H), 1 480, 1 400, 1 170, 1 070, 1 050, 1 000, 910, 880, 850, 790, 720, 510 (Au–P),

† 5,6-μ-Tricyclohexylphosphineaurio-*nido*-decaborane and triethylammonium 5,6,9,10-μ_4-tricyclohexylphosphineaurio-*nido*-dodecahydrodecaborate.

Supplementary data available: see Instructions for Authors, *J. Chem. Soc., Dalton Trans.*, 1990, Issue 1, pp. xix—xxii.

Table 1. Fractional co-ordinates of refined atoms in [5,6-μ-{AuP(C_6H_{11})$_3$}-*nido*-$B_{10}H_{13}$]

Atom	*x*	*y*	*z*
Au	0.190 44(3)	0.231 300(10)	0.422 80(3)
P	0.182 83(18)	0.139 35(8)	0.328 76(18)
B(1)	0.222 1(9)	0.334 3(4)	0.701 9(10)
B(2)	0.212 1(9)	0.377 4(4)	0.563 6(11)
B(3)	0.357 9(12)	0.380 8(5)	0.717 5(12)
B(4)	0.389 0(9)	0.314 8(5)	0.815 4(10)
B(5)	0.152 6(8)	0.301 9(4)	0.539 9(9)
B(6)	0.231 2(9)	0.330 5(4)	0.451 2(10)
B(7)	0.364 0(10)	0.373 5(5)	0.568 2(11)
B(8)	0.483 2(10)	0.333 4(6)	0.740 9(13)
B(9)	0.456 6(13)	0.262 8(7)	0.757 6(12)
B(10)	0.277 4(10)	0.260 5(5)	0.706 1(11)
C(11)	0.242 5(7)	0.081 5(3)	0.458 5(7)
C(12)	0.162 7(8)	0.083 4(4)	0.535 9(8)
C(13)	0.221 1(8)	0.040 0(4)	0.653 5(8)
C(14)	0.361 9(8)	0.051 2(4)	0.743 9(8)
C(15)	0.440 3(8)	0.047 9(4)	0.667 9(8)
C(16)	0.387 7(7)	0.090 3(4)	0.552 2(8)
C(21)	0.016 0(7)	0.119 5(3)	0.199 3(7)
C(22)	−0.089 7(7)	0.151 5(3)	0.222 9(8)
C(23)	−0.226 8(8)	0.140 4(4)	0.105 5(8)
C(24)	−0.255 3(8)	0.075 0(4)	0.086 0(8)
C(25)	−0.149 0(9)	0.040 8(4)	0.068 8(9)
C(26)	−0.012 7(8)	0.051 8(3)	0.182 4(8)
C(31)	0.291 0(7)	0.138 5(3)	0.251 3(7)
C(32)	0.257 3(8)	0.189 2(4)	0.150 3(8)
C(33)	0.361 0(8)	0.191 0(4)	0.100 4(8)
C(34)	0.370 5(8)	0.132 2(4)	0.043 2(8)
C(35)	0.401 5(8)	0.082 1(4)	0.140 2(8)
C(36)	0.297 0(8)	0.078 2(4)	0.190 3(8)

470, and 310 cm^{-1}. N.m.r.: ^{31}P-{^1H} δ 60.9 (br) p.p.m., ^1H-{^{11}B} δ 2.92, 1.79, 1.77, 1.73, 0.63, 0.51 (all B–H), and −4.80 (B–H–B) p.p.m., ^{11}B-{^1H} δ 3.74 (2 B), −6.38 (1 B), −9.69 (2 B), −10.99 (2 B), −28.18 (1 B), and −31.07 (2 B) p.p.m.

(*b*) *With* KOH. To a stirred suspension of compound (**1a**) (0.300 g, 0.500 mmol) in MeOH (20 cm^3) was added solid KOH (0.080 g, 2.22 mmol). The solution colourised as the suspended solid dissolved. After stirring for *ca.* 18 h the solution was filtered into an aqueous solution of excess of [$N(CH_2Ph)Me_3$]Br to give, after filtration in air, an orange microcrystalline product. (The residue has subsequently been shown to be the double cluster [($B_{10}H_{12}Au$){$AuP(C_6H_{11})_3$}$_3$]).[3] Recrystallisation from CH_2Cl_2–n-hexane afforded red *crystals* of the [$N(CH_2Ph)Me_3$]$^+$ salt of (**2a**) (0.161 g, 72%), identified by ^{31}P-{^1H} and ^{11}B-{^1H} n.m.r. spectroscopies.

Deprotonation of [5,6-μ-{$AuP(C_6H_4Me$-2)$_3$}-*nido*-$B_{10}H_{13}$], (**1b**). Deprotonation using NEt_3 followed the above procedure, except that compound (**1b**) is soluble in CH_2Cl_2 in amounts typically used. The [$N(CH_2Ph)Me_3$]$^+$ salt of [*nido*-{$AuP(C_6H_4$-Me-2)$_3$}$B_{10}H_{12}$]$^-$, (**2b**), was obtained as red *crystals* in 82% yield (Found: C, 45.2; H, 7.00; N, 2.40. $C_{27}H_{49}AuB_{10}NP$ requires C, 44.8; H, 6.85; N, 1.95%).

Stoicheiometric protonation of the [$NHEt_3$]$^+$ *salt of* (**2a**). The [$NHEt_3$]$^+$ salt of (**2a**) (0.323 g, 0.462 mmol) was dissolved in CH_2Cl_2 (20 cm^3). To this stirred solution was added CF_3CO_2H (0.460 mmol) (standard solution in CH_2Cl_2). The solution immediately decolourised to very pale yellow. Prompt removal of solvent *in vacuo* afforded a very pale yellow *solid*. ^{31}P-{^1H} N.m.r. spectroscopy of a solution of this showed (**1a**) to be the only phosphorus-containing species present.

Reaction of compound (**1a**) *with* HCl. Compound (**1a**) (0.450 g, 0.752 mmol) was suspended in CH_2Cl_2 (20 cm^3) and cooled to 0 °C. Hydrogen chloride gas was bubbled through this suspension for 30 min. The gas flow was stopped and the product stirred for 24 h at room temperature. Removal of solvent *in vacuo* gave a colourless *crystalline solid*, identified by ^{31}P-{^1H} and ^{11}B-{^1H} n.m.r. spectroscopies as a mixture of [$AuCl\{P(C_6H_{11})_3\}$] and $B_{10}H_{14}$.

Crystallographic Studies.—All measurements were made on an Enraf-Nonius CAD4 diffractometer equipped for low-temperature work and operating with graphite-monochromated Mo-K_α *X*-radiation, $\bar{\lambda}$ = 0.710 69 Å.

Compound (**1a**). The structure of this species has previously been reported,[1] based on a limited, room temperature data set. We have recollected data to higher resolution at 185 ± 1 K.

Crystal data. a = 11.598(3), b = 22.459(4), c = 11.394 3(21) Å, β = 118.003(19)°, U = 2 620.6 $Å^3$, from 25 centred reflections, 15 < θ < 16°.

Data collection and processing. ω—2θ scans, ω scan width 0.8 + 0.35tanθ. Variable scan speeds, 0.824—2.354° min^{-1}. 6 783 Unique data (1 ⩽ θ ⩽ 28°, + h + k ± l), yielding 5 442 reflections with $F \geqslant 2\sigma(F)$. Slight crystal decay noted and corrected.

Refinement. Previously determined model used as starting point in refinement. Empirical[4] absorption correction applied after isotropic convergence. Data weighted according to $w^{-1} = [\sigma^2(F) + g(F)^2]$, g = 0.000 311. All non-H atoms refined anisotropically. Cyclohexyl and cage terminal H atoms set in calculated positions (C–H 1.08 Å, B–H 1.18 Å[5]). Bridging H atoms located from ΔF synthesis and included in F_c calculations, but not refined. Isotropic group thermal parameters for cyclohexyl and cage H atoms, 0.039(4) and 0.076(10) $Å^2$ respectively at convergence. Maximum and minimum residues in final ΔF map 0.455 and −0.621 e $Å^{-3}$. R = 0.0458, R' = 0.0668, S = 1.524, with a data:variable ratio >20:1. Co-ordinates of refined atoms are in Table 1.

The [$NHEt_3$]$^+$ *salt of* (**2a**). All measurements at 291 ± 1 K.

Crystal data. $C_{24}H_{61}AuB_{10}NP$, M = 699.8, monoclinic, a = 17.559 8(23), b = 11.692 9(20), c = 18.533(3) Å, β = 116.797(11)°, U = 3 396.5 $Å^3$, by the least-squares refinement of 25 centred reflections, 13 < θ < 15°, space group $P2_1/a$, Z = 4, D_c = 1.368 g cm^{-3}, μ(Mo-K_α) = 43.84 cm^{-1}, F(000) = 1 424.

Data collection and processing. As for (**1a**) except 1 ⩽ θ ⩽ 25°, scan speeds 0.824—2.747° min^{-1}. 6 437 Unique data yielding 4 474 with $F \geqslant 2\sigma(F)$. Very strong pseudo-*C* centring noted.

Structure solution and refinement. Gold atom located from inspection of Patterson synthesis, near-zero y co-ordinate responsible for pseudo-centring. All other non-H atoms from iterative refinement/ΔF syntheses. Absorption correction and weighting scheme as for (**1a**), g = 0.000 634. Gold, P, B, and N atoms refined anisotropically, five cation C atoms equally disordered over pairs of sites. All C atoms refined isotropically, freely in the anion but with one common N–C distance [1.55(1) Å at convergence] and one common C–C distance [1.41(1) Å at convergence] in the cation. Hydrogen atoms terminal to cage located and freely refined, bridge-H atoms constrained to a common B–H distance, 1.30(1) Å at convergence. Group thermal parameters for (idealised) H atoms of C_6H_{11} rings [0.070(5) $Å^2$] and for cage H atoms [0.049(7) $Å^2$]. Maximum peak and minimum trough in final ΔF synthesis 0.733 and −0.607 e $Å^{-3}$. R = 0.0411, R' = 0.0531, S = 1.205. Data: variables better than 16:1. Co-ordinates of refined atoms appear in Table 2. Scattering factors for Au from ref. 6. Those for P, B, N, C, and H inlaid in SHELX 76.[7] Computer programs CADABS,[8] SHELX 76, DIFABS,[4] CALC,[5] and EASY-ORTEP.[9]

Additional material available from the Cambridge Crystal-

Table 2. Fractional co-ordinates of refined atoms in $[NHEt_3]^+$ $[\{AuP(C_6H_{11})_3\}B_{10}H_{12}]^-$

Atom	*x*	*y*	*z*
Au	0.147 840(20)	−0.008 840(20)	0.261 470(20)
P	0.215 82(12)	0.004 06(14)	0.181 12(11)
B(1)	0.026 9(6)	−0.031 6(8)	0.367 2(6)
B(2)	0.024 8(6)	−0.174 9(8)	0.333 3(6)
B(3)	−0.064 5(6)	−0.083 8(8)	0.278 9(6)
B(4)	−0.036 4(6)	0.062 1(8)	0.288 0(6)
B(5)	0.117 1(6)	−0.084 9(8)	0.359 4(6)
B(6)	0.086 6(6)	−0.188 3(7)	0.282 8(6)
B(7)	−0.026 8(7)	−0.175 9(8)	0.228 1(6)
B(8)	−0.070 8(6)	−0.010 3(8)	0.194 6(6)
B(9)	0.013 0(6)	0.096 7(7)	0.228 6(6)
B(10)	0.075 7(6)	0.066 2(7)	0.326 8(5)
C(11)	0.333 4(5)	0.005 9(6)	0.238 8(4)
C(12)	0.364 2(6)	0.050 6(9)	0.324 1(6)
C(13)	0.460 2(7)	0.038 6(9)	0.374 4(7)
C(14)	0.506 2(7)	0.092 4(9)	0.330 4(6)
C(15)	0.478 3(7)	0.049 9(9)	0.251 3(6)
C(16)	0.383 0(5)	0.060 4(8)	0.198 2(5)
C(21)	0.188 4(5)	−0.120 5(6)	0.112 6(5)
C(22)	0.219 3(5)	−0.232 1(6)	0.160 4(5)
C(23)	0.184 3(6)	−0.335 2(7)	0.106 3(5)
C(24)	0.204 5(6)	−0.331 9(7)	0.035 6(5)
C(25)	0.174 8(6)	−0.219 2(7)	−0.011 7(5)
C(26)	0.214 2(5)	−0.117 6(7)	0.043 7(5)
C(31)	0.184 1(5)	0.132 8(6)	0.115 6(4)
C(32)	0.197 1(6)	0.240 1(7)	0.167 2(5)
C(33)	0.167 7(7)	0.349 8(8)	0.117 0(6)
C(34)	0.074 4(7)	0.336 5(8)	0.049 2(6)
C(35)	0.064 0(7)	0.231 4(7)	−0.001 7(6)
C(36)	0.091 5(5)	0.124 1(6)	0.050 9(5)
N	0.302 3(5)	0.581 5(6)	0.458 4(5)
C(11a)	0.315 8(12)	0.709 2(13)	0.442 8(15)
C(11b)	0.362 3(17)	0.651 6(22)	0.434 3(9)
C(12b)	0.372(3)	0.769 7(22)	0.427 0(23)
C(12a)	0.405 2(10)	0.726 6(14)	0.474 4(10)
C(21a)	0.208 4(9)	0.569 4(17)	0.442 4(10)
C(21b)	0.234 6(12)	0.659 5(14)	0.466 0(13)
C(22t)	0.188 7(8)	0.608 8(9)	0.504 1(7)
C(31a)	0.319 4(16)	0.497 1(17)	0.402 3(13)
C(31b)	0.262 2(16)	0.471 8(18)	0.410 9(19)
C(32a)	0.246 7(20)	0.470(3)	0.329 9(19)
C(32b)	0.317 5(15)	0.393 5(18)	0.401 4(15)

Table 3. Parameters used in EHMO calculations

Orbital	H_{ii}/eV	ζ_1
H(1*s*)	−13.60	1.30
B(2*s*)	−15.20	1.30
B(2*p*)	−8.50	1.30
P(3*s*)	−18.60	1.60
P(3*p*)	−14.00	1.60
P(3*d*)	−7.00	1.40
Au(6*s*)	−9.22	2.60
Au(6*p*)	−4.27	2.58
Au(5*d*)	−11.85	6.16*

* $\zeta_2 = 2.73, c_1 = 0.648\ 55, c_2 = 0.539\ 46$.

lographic Data Centre comprises H-atom co-ordinates, thermal parameters, and remaining bond lengths and angles.

Molecular Orbital Calculations.—Extended Hückel molecular orbital (EHMO) calculations were carried out using a locally modified version of ICON8,[10] H_{ii} values and orbital exponents given in Table 3, and the modified H_{ij} formula.[11] Where noted

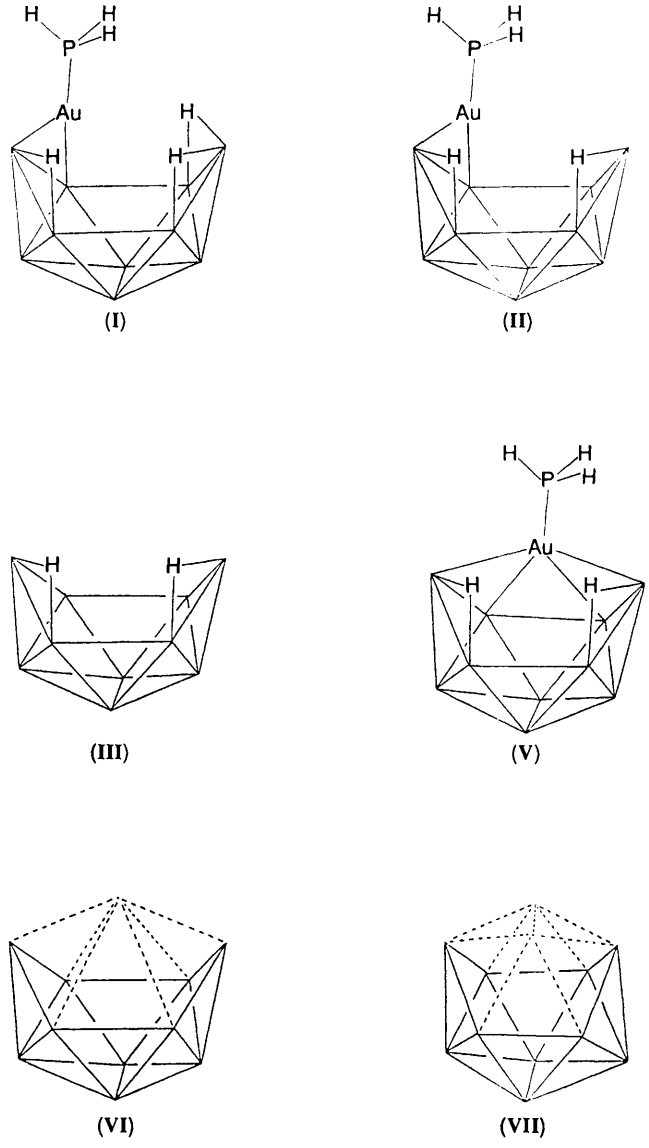

Figure 1. Line diagrams of the model compounds or fragments (I)—(III) and (V) (terminal H atoms not included), and of *nido* 10-vertex and *arachno* 10-vertex polyhedra [(VI) and (VII) respectively] showing, in addition, the positions of missing vertices at the points of intersection of dashed connectivities

calculations were charge-iterated at the simplest level, *i.e.* $H_{ii} = H_{ii}^{\circ}$ + (sense) × (charge).[10] The models used in these calculations were taken from the experimental geometry of $B_{10}H_{14}$,[12] slightly adjusted to full C_{2v} symmetry, and a gold phosphine fragment was constructed with Au–P 2.30 Å, P–H 1.42 Å, H–Au–P 109.47°.

The following model compounds or fragments were examined: (I) [5,6-μ-($AuPH_3$)-*nido*-$B_{10}H_{13}$], (II) [9,10]-deprotonated (I), (III) $\{B_{10}H_{12}\}^{2-}$ ($B_{10}H_{14}$ minus 5,6-μ-H^+ and 9,10-μ-H^+), (IV) $\{AuPH_3\}^+$, and (V) [5,6,9,10-μ_4-($AuPH_3$)-*nido*-$B_{10}H_{12}$]$^-$. In (I) the $\{AuPH_3\}$ fragment was attached to the cage in the same orientation as that observed crystallographically in compound (**1a**), with Au–B(5) 2.2540, Au–B(6) 2.4074 Å. In (V) the gold atom was set 1.70 Å above the ligating B_4 plane [Au–B(5) 2.3586, Au–B(6) 2.4901 Å], and two different inclinations of the Au–P vector to the B_4 plane were considered, normal and 26° [PH_3 tilted towards the B(6)B(7)B(8)B(9) face].

Table 4. Bond lengths (Å) and angles (°) for the refined atoms in [5,6-μ-{AuP(C_6H_{11})$_3$}-*nido*-$B_{10}H_{13}$]

Au–P	2.309 1(21)	B(3)–B(4)	1.788(17)	B(9)–B(10)	1.877(19)	C(21)–C(26)	1.550(11)
Au–B(5)	2.245(10)	B(3)–B(7)	1.743(17)	P–C(11)	1.842(8)	C(22)–C(23)	1.543(12)
Au–B(6)	2.270(10)	B(3)–B(8)	1.717(19)	P–C(21)	1.854(8)	C(23)–C(24)	1.499(13)
B(1)–B(2)	1.807(15)	B(4)–B(8)	1.720(18)	P–C(31)	1.842(8)	C(24)–C(25)	1.542(14)
B(1)–B(3)	1.828(17)	B(4)–B(9)	1.701(19)	C(11)–C(12)	1.550(12)	C(25)–C(26)	1.521(13)
B(1)–B(4)	1.806(15)	B(4)–B(10)	1.789(16)	C(11)–C(16)	1.525(11)	C(31)–C(32)	1.533(12)
B(1)–B(5)	1.785(14)	B(5)–B(6)	1.770(14)	C(12)–C(13)	1.534(13)	C(31)–C(36)	1.539(12)
B(1)–B(10)	1.770(16)	B(5)–B(10)	1.994(15)	C(13)–C(14)	1.487(13)	C(32)–C(33)	1.554(13)
B(2)–B(3)	1.777(17)	B(6)–B(7)	1.776(15)	C(14)–C(15)	1.525(13)	C(33)–C(34)	1.500(13)
B(2)–B(5)	1.803(14)	B(7)–B(8)	2.010(18)	C(15)–C(16)	1.505(12)	C(34)–C(35)	1.496(13)
B(2)–B(6)	1.751(15)	B(8)–B(9)	1.643(20)	C(21)–C(22)	1.550(11)	C(35)–C(36)	1.566(13)
B(2)–B(7)	1.740(16)						
P–Au–B(5)	158.8(3)	B(1)–B(4)–B(3)	61.1(6)	B(4)–B(9)–B(8)	61.9(8)	C(11)–C(16)–C(15)	113.0(7)
P–Au–B(6)	154.7(3)	B(1)–B(4)–B(10)	59.0(6)	B(4)–B(9)–B(10)	59.8(7)	P–C(21)–C(22)	111.4(5)
B(5)–Au–B(6)	46.2(4)	B(3)–B(4)–B(8)	58.6(7)	B(1)–B(10)–B(4)	61.0(6)	P–C(21)–C(26)	114.7(5)
B(2)–B(1)–B(3)	58.5(6)	B(8)–B(4)–B(9)	57.4(8)	B(1)–B(10)–B(5)	56.3(6)	C(22)–C(21)–C(26)	109.6(6)
B(2)–B(1)–B(5)	60.2(6)	B(9)–B(4)–B(10)	65.0(7)	B(4)–B(10)–B(9)	55.2(7)	C(21)–C(22)–C(23)	110.6(7)
B(3)–B(1)–B(4)	58.9(6)	Au–B(5)–B(6)	67.7(5)	Au–P–C(11)	109.88(25)	C(22)–C(23)–C(24)	110.7(7)
B(4)–B(1)–B(10)	60.0(6)	B(1)–B(5)–B(2)	60.5(6)	Au–P–C(21)	112.49(25)	C(23)–C(24)–C(25)	111.9(8)
B(5)–B(1)–B(10)	68.2(6)	B(1)–B(5)–B(10)	55.5(5)	Au–P–C(31)	110.2(3)	C(24)–C(25)–C(26)	112.6(8)
B(1)–B(2)–B(3)	61.3(6)	B(2)–B(5)–B(6)	58.7(6)	C(11)–P–C(21)	109.1(3)	C(21)–C(26)–C(25)	110.0(7)
B(1)–B(2)–B(5)	59.3(6)	Au–B(6)–B(5)	66.2(4)	C(11)–P–C(31)	107.1(4)	P–C(31)–C(32)	111.2(6)
B(3)–B(2)–B(7)	59.4(7)	B(2)–B(6)–B(5)	61.6(6)	C(21)–P–C(31)	107.9(4)	P–C(31)–C(36)	114.3(6)
B(5)–B(2)–B(6)	59.7(6)	B(2)–B(6)–B(7)	59.1(6)	P–C(11)–C(12)	109.7(5)	C(32)–C(31)–C(36)	111.3(7)
B(6)–B(2)–B(7)	61.1(6)	B(2)–B(7)–B(3)	61.3(7)	P–C(11)–C(16)	110.2(5)	C(31)–C(32)–C(33)	109.0(7)
B(1)–B(3)–B(2)	60.2(6)	B(2)–B(7)–B(6)	59.7(6)	C(12)–C(11)–C(16)	110.9(6)	C(32)–C(33)–C(34)	111.3(7)
B(1)–B(3)–B(4)	59.9(6)	B(3)–B(7)–B(8)	53.9(7)	C(11)–C(12)–C(13)	110.0(7)	C(33)–C(34)–C(35)	112.5(8)
B(2)–B(3)–B(7)	59.2(7)	B(3)–B(8)–B(4)	62.7(7)	C(12)–C(13)–C(14)	112.9(8)	C(34)–C(35)–C(36)	110.6(7)
B(4)–B(3)–B(8)	58.7(7)	B(3)–B(8)–B(7)	55.1(6)	C(13)–C(14)–C(15)	110.6(7)	C(31)–C(36)–C(35)	108.8(7)
B(7)–B(3)–B(8)	71.0(8)	B(4)–B(8)–B(9)	60.7(8)	C(14)–C(15)–C(16)	111.2(7)		

Line diagrams of the above models, and of other species or fragments discussed below, are presented in Figure 1.*

Results and Discussion

Molecular and Electronic Structures of Compound (**1**).—The previous (room temperature) structural determination of compounds (**1a**) and (**1b**) suggested a possible interaction between the gold atom and the B(9)H(9,10)B(10) bridge system, similar in type to the weak Hg · · · BHB interaction previously studied by Finster and Grimes[13] in carbacobaltamercuraboranes. Firm structural evidence for such an interaction in the present compound derives from the more accurate, low-temperature redetermination of (**1a**). Table 4 lists selected molecular parameters, and Figure 2 views the molecule. The key result of the low temperature study is that the gold atom bridges the B(5)–B(6) connectivity asymmetrically (more so than does μ–H in $B_{10}H_{14}$[12]), favouring B(5). Thus Au–B(5) < Au–B(6), Δ

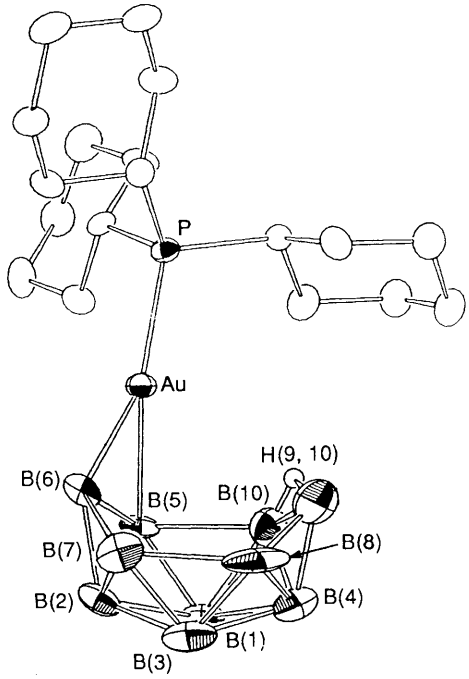

Figure 2. Molecular structure of [5,6-μ-{AuP(C_6H_{11})$_3$}-*nido*-$B_{10}H_{13}$] (**1a**) from the low-temperature diffraction experiment. Thermal ellipsoids drawn at the 50% probability level, except for H(9,10) (the only hydrogen atom shown, for clarity) which has an artificial radius of 0.1 Å. All boron atoms carry terminal H atoms, and there are μ-H atoms bridging the B(6)–B(7) and B(8)–B(9) connectivities

* At the suggestion of a referee we have checked the validity of our theoretical approach by repeating several calculations using experimentally derived models and the highest level of charge iteration available, $H_{ii} = -$VSIE(Q), using nine VSIE(Q) functions for gold, six each for phosphorus and boron, and three for hydrogen. For computational expediency PR_3 is still modelled by PH_3, and because they were not refined in the crystallographic study, μ-H atoms for (**1a**) were set in idealised positions. The key results are: (*i*) [5,6-μ-($AuPH_3$)-*nido*-$B_{10}H_{13}$], maximum a.o. overlap integrals ⟨Au/B(5,6)⟩ 0.32, ⟨Au/B(10)⟩ 0.16, ⟨Au/H(9,10)⟩ 0.13, ⟨Au/H(5,6)⟩ 0.16, all other ⟨Au/B⟩ ⟨0.1, all other ⟨Au/H⟩ ⟨0.1; (*ii*) [5,6-μ-($AuPH_3$)-*nido*-$B_{10}H_{12}$]$^-$ (9,10-deprotonated), h.o.m.o. localised on (descending order) B(10) ≈ B(9) > B(6) > B(2) ≈ B(7) ≈ B(5) ≈ Au; the contributions on B(10), B(9), B(6), and Au are essentially as drawn in Figure 3(*b*); (*iii*) [5,6,9,10-μ$_4$-($AuPH_3$)-*nido*-$B_{10}H_{12}$]$^-$, {$B_{10}H_{12}$}$^{2-}$ fragment transfers between 0.6 and 0.8e to {$AuPH_3$}$^+$ fragment, occupation of l.u.m.o. of {$B_{10}H_{12}$}$^{2-}$ fragment in molecule only 0.046e. The broad similarity of these results with those reported in the body of the paper suggest that the latter are *qualitatively* reasonable. VSIE(Q) = Valence state ionisation energy of orbital *i* when atom has total charge *Q*.

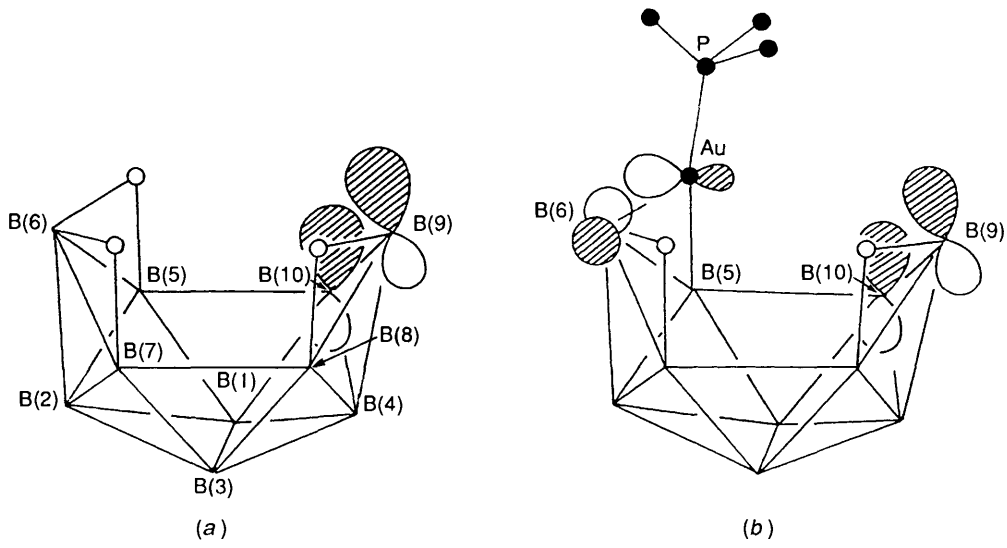

Figure 3. H.o.m.o.s of (*a*) $[B_{10}H_{13}]^-$, derived from $B_{10}H_{14}$ by removal of the formerly bridging proton $H^+(9,10)$, and (*b*) model compound (**II**). ○ = μ-H atom, ● = atom of μ-$AuPH_3$ unit

Table 5. Bond lengths (Å) and angles (°) for the refined atoms in the $[\{AuP(C_6H_{11})_3\}B_{10}H_{12}]^-$ anion

Au–P	2.295 2(20)	B(2)–B(6)	1.729(14)	B(8)–B(9)	1.813(15)	C(22)–C(23)	1.510(13)
Au–B(5)	2.294(10)	B(2)–B(7)	1.740(15)	B(9)–B(10)	1.687(14)	C(23)–C(24)	1.504(13)
Au–B(6)	2.469(10)	B(3)–B(4)	1.763(15)	P–C(11)	1.848(8)	C(24)–C(25)	1.537(13)
Au–B(9)	2.490(10)	B(3)–B(7)	1.746(15)	P–C(21)	1.848(8)	C(25)–C(26)	1.518(13)
Au–B(10)	2.285(10)	B(3)–B(8)	1.743(15)	P–C(31)	1.855(8)	C(26)–C(21)	1.535(12)
B(1)–B(2)	1.784(15)	B(4)–B(8)	1.770(15)	C(11)–C(12)	1.514(14)	C(31)–C(32)	1.530(13)
B(1)–B(3)	1.804(15)	B(4)–B(9)	1.729(14)	C(12)–C(13)	1.521(16)	C(32)–C(33)	1.531(15)
B(1)–B(4)	1.765(15)	B(4)–B(10)	1.766(14)	C(13)–C(14)	1.518(16)	C(33)–C(34)	1.559(16)
B(1)–B(5)	1.767(15)	B(5)–B(6)	1.754(15)	C(14)–C(15)	1.411(16)	C(34)–C(35)	1.508(15)
B(1)–B(10)	1.783(14)	B(5)–B(10)	1.903(14)	C(15)–C(16)	1.516(15)	C(35)–C(36)	1.528(13)
B(2)–B(3)	1.785(15)	B(6)–B(7)	1.786(15)	C(16)–C(11)	1.524(12)	C(36)–C(31)	1.528(11)
B(2)–B(5)	1.804(15)	B(7)–B(8)	2.074(16)	C(21)–C(22)	1.533(12)		
P–Au–B(5)	156.3(3)	B(4)–B(3)–B(8)	60.7(6)	B(4)–B(8)–B(9)	57.7(6)	C(13)–C(14)–C(15)	113.1(10)
P–Au–B(6)	123.45(24)	B(7)–B(3)–B(8)	72.9(7)	Au–B(9)–B(10)	62.9(5)	C(14)–C(15)–C(16)	114.2(9)
P–Au–B(9)	121.60(24)	B(1)–B(4)–B(3)	61.5(6)	B(4)–B(9)–B(8)	59.9(6)	C(11)–C(16)–C(15)	110.9(8)
P–Au–B(10)	153.3(3)	B(1)–B(4)–B(10)	60.7(6)	B(4)–B(9)–B(10)	62.2(6)	P–C(21)–C(22)	111.1(6)
B(5)–Au–B(6)	43.0(4)	B(3)–B(4)–B(8)	59.1(6)	Au–B(10)–B(5)	65.7(4)	P–C(21)–C(26)	118.1(6)
B(5)–Au–B(10)	49.1(4)	B(8)–B(4)–B(9)	62.4(6)	Au–B(10)–B(9)	76.0(5)	C(22)–C(21)–C(26)	109.8(7)
B(9)–Au–B(10)	41.1(3)	B(9)–B(4)–B(10)	57.7(6)	B(1)–B(10)–B(4)	59.7(6)	C(21)–C(22)–C(23)	111.4(7)
B(2)–B(1)–B(3)	59.7(6)	Au–B(5)–B(6)	73.8(5)	B(1)–B(10)–B(5)	57.2(5)	C(22)–C(23)–C(24)	111.8(8)
B(2)–B(1)–B(5)	61.1(6)	Au–B(5)–B(10)	65.2(4)	B(4)–B(10)–B(9)	60.1(6)	C(23)–C(24)–C(25)	111.5(8)
B(3)–B(1)–B(4)	59.2(6)	B(1)–B(5)–B(2)	59.9(6)	Au–P–C(11)	113.4(3)	C(24)–C(25)–C(26)	110.5(8)
B(4)–B(1)–B(10)	59.7(6)	B(1)–B(5)–B(10)	58.0(6)	Au–P–C(21)	110.1(3)	C(21)–C(26)–C(25)	109.3(7)
B(5)–B(1)–B(10)	64.8(6)	B(2)–B(5)–B(6)	58.1(6)	Au–P–C(31)	112.8(3)	P–C(31)–C(32)	109.9(6)
B(1)–B(2)–B(3)	60.7(6)	Au–B(6)–B(5)	63.2(5)	C(11)–P–C(21)	106.5(4)	P–C(31)–C(36)	110.0(5)
B(1)–B(2)–B(5)	59.0(6)	B(2)–B(6)–B(5)	62.4(6)	C(11)–P–C(31)	107.2(4)	C(32)–C(31)–C(36)	110.6(7)
B(3)–B(2)–B(7)	59.4(6)	B(2)–B(6)–B(7)	59.3(6)	C(21)–P–C(31)	106.4(4)	C(31)–C(32)–C(33)	113.1(8)
B(5)–B(2)–B(6)	59.5(6)	B(2)–B(7)–B(3)	61.6(6)	P–C(11)–C(12)	112.8(6)	C(32)–C(33)–C(34)	110.5(9)
B(6)–B(2)–B(7)	62.0(6)	B(2)–B(7)–B(6)	58.7(6)	P–C(11)–C(16)	117.3(6)	C(33)–C(34)–C(35)	111.9(9)
B(1)–B(3)–B(2)	59.6(6)	B(3)–B(7)–B(8)	53.4(6)	C(12)–C(11)–C(16)	110.8(7)	C(34)–C(35)–C(36)	110.8(8)
B(1)–B(3)–B(4)	59.3(6)	B(3)–B(8)–B(4)	60.2(6)	C(11)–C(12)–C(13)	112.6(9)	C(31)–C(36)–C(35)	111.4(7)
B(2)–B(3)–B(7)	59.0(6)	B(3)–B(8)–B(7)	53.6(6)	C(12)–C(13)–C(14)	110.1(9)		

0.025 Å, Δ/σ 1.79, and P–Au–B(5) > P–Au–B(6), Δ 4.1°, Δ/σ 10.25.

Further support for an Au • • • B(9)H(9,10)B(10) interaction, and some indication of its nature, derives from the results of EHMO calculations and from the Mössbauer spectrum of (**Ia**). In the model compound (**I**) the maximum overlap integrals between gold 6*s* and 6*p* atomic orbitals (a.o.s) and a.o.s of B(5) and B(6) are of the order of 0.33. In addition, integrals of *ca.* 0.12 and 0.19 occur between the valence a.o.s of gold and those of B(10) and H(9,10) respectively. All other gold–boron overlap integrals are <0.1, as are all other gold–hydrogen integrals except those involving H(5) and H(6). Figure 3 shows plots of the highest occupied m.o.s (h.o.m.o.s) of (*a*) 9,10-deprotonated $B_{10}H_{14}$, and (*b*) of (**II**). Whilst the h.o.m.o. of $[B_{10}H_{13}]^-$ is heavily localised above the B(9)–B(10) connectivity, that of (**II**) is more delocalised, also having significant contributions from B(6) and Au. The contribution on gold is an *sp* hybrid, mixed so as to reinforce the *p* a.o. towards B(6), with which it is in

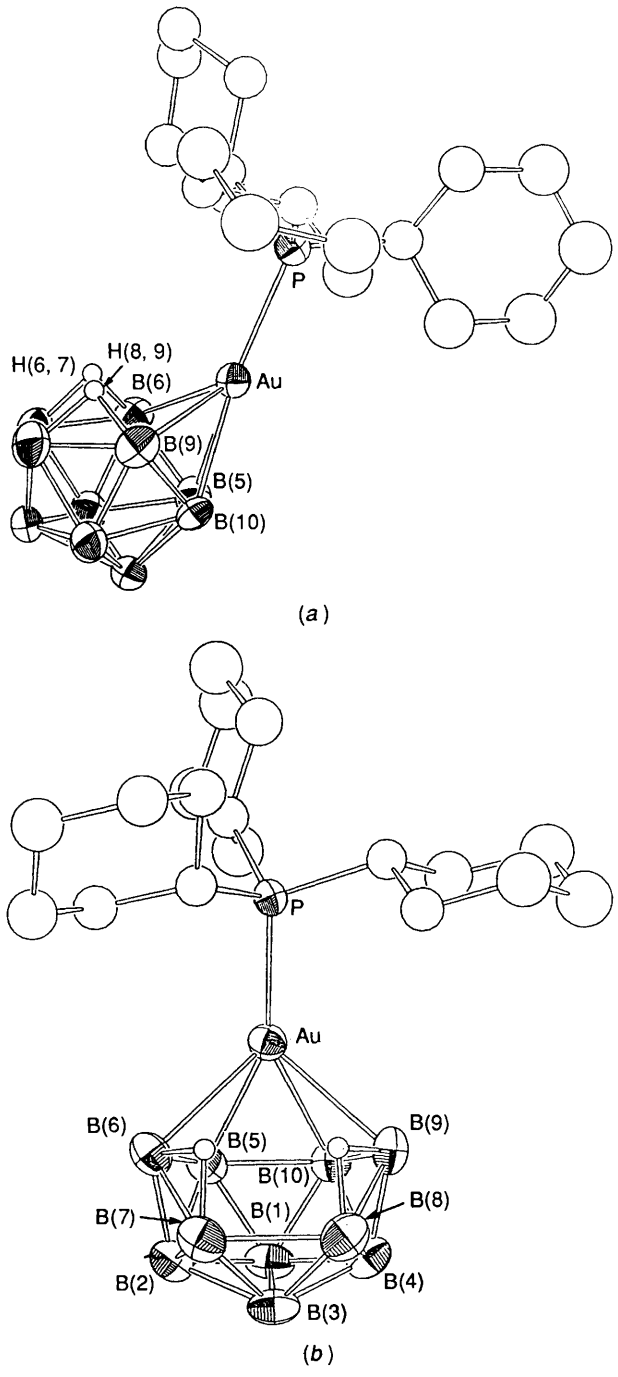

Figure 4. Molecular structure of $[\mu_4\text{-}\{AuP(C_6H_{11})_3\}\text{-}nido\text{-}B_{10}H_{12}]^-$ as found crystallographically as its $[NHEt_3]^+$ salt. Thermal ellipsoids as in Figure 2. For clarity only the μ-H atoms are shown. Every boron atom has a terminal hydrogen attached

phase. Importantly, in terms of the present discussion, the smaller lobe of the gold hybrid orbital points towards the B(9)–B(10) edge, and is in phase with the orbital contributions from B(9) and B(10). Protonation of (**II**) therefore means that the B(9)H(9,10)B(10) bridge system must have real, albeit small, bonding interaction with the μ-5,6-gold atom. In localised terms[14] this converts a three-centre two-electron bridge (BHB) into a four-centre two-electron one (BHAuB).

The ^{197}Au Mössbauer spectrum of (**1a**) gives isomer shift (i.s.) (Au) = 4.51 mm s^{-1} and quadrupole splitting (q.s.) = 9.01 mm s^{-1}. These parameters lie in the same region as those for conventional linearly co-ordinated gold(I) compounds.[15] Although the gold atom cannot be regarded as two-co-ordinate, this observation confirms that it effectively employs only two orbitals in bonding to the phosphine and the $\{B_{10}\}$ cluster. Thus, the phosphine–gold unit is indeed isolobal with the H atom which it replaces, as has been found also for metal–cluster compounds containing gold.[16,17] Such systems are better regarded as having an *orbital number* of two, rather than being pseudo-two-co-ordinate. There are, however, two significant differences from the metal cluster data. First, the values of the parameters for (**1a**) are considerably greater than those of the metal clusters. Higher values are normally associated with clusters in which the gold atom has a low connectivity, but the present values indicate that the population of the $6sp_z$ hybrid is relatively high [for the present purposes, z is the direction from Au to the midpoint of B(5)–B(6)]. From the point of view of the gold atom, the $\{B_{10}H_{13}\}$ cluster acts as a 'soft' ligand comparable to SMe_2 or $AsPh_3$. Secondly, the parameters lie on the upper edge of the band of values. For conventional compounds this often indicates additional, weak bonding interactions as, for instance, in $[AuL(L\text{–}L)]^+$ (L = tetrahydrothiophene or PPh_3; L–L = 2,2′-bipyridine or 1,10-phenanthroline][18,19] and other related systems;[15] fully three-co-ordinate compounds show q.s. values similar to analogous two-co-ordinate systems but have substantially lower i.s. values. In both cases the lowering of the i.s. reflects increased population of the gold 6*p* orbitals. Thus, the Mössbauer data are fully consistent with an Au · · · B(9)H(9,10)B(10) interaction.

Synthesis, Structure, Bonding, and Reactivity of Compound (**2a**).—Deprotonation of (**1a**) with either NEt_3 or KOH and of (**1b**) with NEt_3 affords the appropriate salt of the red compounds (**2a**) or (**2b**) in high yield. The ^{11}B-{^{1}H} and ^{1}H-{^{11}B} n.m.r. spectra of compounds (**2**) are fully consistent with species having C_s molecular symmetry. A crystallographic analysis of the $[NHEt_3]^+$ salt of (**2a**) was undertaken unambiguously to prove the molecular structure. Figure 4 shows two different views of the anion, and Table 5 lists important molecular parameters. Figure 4(*a*) clearly shows that the Au–P vector is not normal to the B(6)B(5)B(10)B(9) plane, rather it is inclined 25.9° towards the open face defined by Au, B(6), B(7), B(8), and B(9).

Superficial consideration of the structure of (**2a**) suggests a *nido*-icosahedral architecture in which the gold atom is a vertex in an open five-atom face, implying that the $\{B_{10}\}$ moiety is present as the *arachno* fragment $\{B_{10}H_{12}\}^{4-}$, and thus that the formal oxidation state of the gold atom in (**2**) is +3. However, we do not believe this to be the most appropriate description. Conventional electron-counting procedures[20] applied to heteroboranes containing co-ordinatively unsaturated late transition elements frequently have little realistic validity,[21] and consequently we have not used them to derive the formal electronic cluster contribution (*i.e.* formal oxidation state) of the gold atom in (**2**). Rather, the Mössbauer parameters determined for (**2a**), i.s.(Au) 3.68 and q.s. 8.13 mm s^{-1}, clearly establish the Au oxidation state as +1,[15] this in turn implying that in (**2a**) the $\{B_{10}\}$ fragment is present as $\{B_{10}H_{12}\}^{2-}$, *i.e.* a *nido* 10-vertex fragment.

The precise description of the $\{B_{10}\}$ part of compound (**2**) is important because *nido*-10 vertex (**VI**) and *arachno*-10 vertex (**VII**) polyhedra are structurally very little different[22] (in fact the connectivity pattern of the vertices is *exactly* the same), in spite of the fact that the latter has an additional skeletal electron pair. Kennedy[23] has pointed out that in metallaboranes in which the $\{B_{10}\}$ unit is present as a decaboranyl fragment long B(5)–B(10) and B(7)–B(8) distances are retained, and these distances in (**2a**) [1.903(14) and 2.074(16) Å respectively (these are discussed in relation to each other below)] are certainly in broad

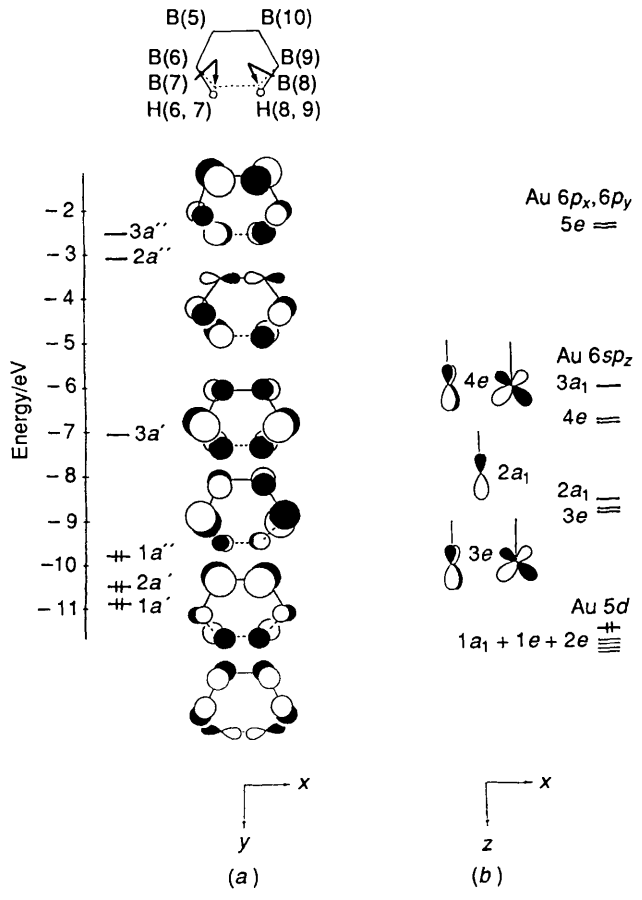

Figure 5. (*a*) The frontier orbitals of (**III**) drawn from a position above the B(6)B(5)B(10)B(9) plane. Contributions from these atoms and from B(7) and B(8) are shown. With respect to B(6)B(5)B(10)B(9), B(7) and B(8) lie 1.3 Å below the plane whilst H(6,7) and H(8,9) are almost exactly in the plane. (*b*) Important orbitals of the $\{AuPH_3\}^+$ fragment, (**IV**), as given by an EHMO calculation in which phosphorus 3*d* a.o.s were included. The $1a_1$, 1*e*, 2*e*, $3a_1$, and 5*e* orbitals have been described previously.[31] Orbitals 3*e*, $2a_1$, and 4*e* are mainly phosphorus-based, but have significant amounts of gold character, as shown. The view in Figure 5(*b*) is orthogonal to that in 5(*a*)

agreement with this. We prefer, however, to utilise a technique for differentiation between the two alternatives (*nido* and *arachno* $\{B_{10}\}$ fragments) that considers the *whole* of the $\{B_{10}\}$ cage, not simply selected molecular parameters. One of the routines of the computer program CALC[5] allows calculation of the root mean square (r.m.s.) misfit of two molecular fragments established crystallographically. The lower the value of this parameter, the better is the fit. The r.m.s. misfit of the $\{B_{10}\}$ fragment of (**2a**) *versus* that of $B_{10}H_{14}$[12] is 0.048 Å, *versus* that of $[B_{10}H_{14}]^{2-}$[24] (an *arachno* 10-vertex species) is 0.120 Å, and *versus* the appropriate *arachno* $\{B_{10}\}$ fragment of $[B_{11}H_{13}]^{2-}$[25] is 0.172 Å. Hence this analysis clearly indicates that the $\{B_{10}\}$ moiety of (**2a**) is better described as $\{B_{10}H_{12}\}^{2-}$.

Accordingly, both the Mössbauer data and the structural comparisons lead to the conclusion that in compound (**2a**) the $\{B_{10}\}$ polyhedron is most accurately described as decaborane-like, *i.e.* a *nido* 10-vertex (12 skeletal electron pair) species in which the gold(I) atom is formally *not* a polyhedral vertex, rather it occupies a μ_4 trapezoidal bridging site over the B(6)B(5)B(10)B(9) face. For this reason we have numbered the cage atoms in (**2a**) as in decaborane. Analysis of the structure of (**2a**) in this way allows an important comment on the differences in bonding capability of an H atom and a (formally isolobal) $\{AuPR_3\}$ fragment, in that 9,10-deprotonation of $B_{10}H_{14}$ affords $[B_{10}H_{13}]^-$ in which the μ-5,6-H atom remains as a simple edge bridge,[26,27] whereas deprotonation of (**1**) yields (**2**) in which the μ-5,6-Au^IPR_3 function slips across from μ to μ_4. Although we have not constructed a Walsh diagram to model this slipping, stabilisation of the h.o.m.o. of (**II**) is clearly going to be an important contributory factor.

In compound (**2a**) the gold atom is 0.717 Å above the best (least-squares) plane through B(6), B(7), B(8), and B(9). This is additional evidence that the $\{AuB_{10}\}$ fragment of (**2**) is not best regarded as *nido*-icosahedral, since in such species as $[(B_{10}H_{12})Au(B_{10}H_{12})]^-$[28] and $[(B_{10}H_{12}Au)(AuPR_3)_4(AuB_{10}H_{12})]$[29] (R = Et or Ph) corresponding displacements are only of the order of 0.4—0.5 Å. However, further to probe the nature of the gold-cage bonding in (**2**) requires consideration of the frontier orbitals of the fragments *nido*-$\{B_{10}H_{12}\}^{2-}$ (**III**) and $\{AuPH_3\}^+$ (**IV**).

EHMO calculation affords frontier orbitals of (**III**) shown in Figure 5(*a*). There is an obvious crude relationship between these orbitals and the π m.o.s of benzene,[30] but in view of the fact that an incoming metal fragment is ligated by a four-atom face [B(6)B(5)B(10)B(9)] the analogy we prefer to develop is that with the π m.o.s of *cis*-butadiene.[30] Generally, this analogy is quite good, although subtle differences in orientations and coefficients of the contributing a.o.s are apparent, and in particular the occupied *a'* and unoccupied *a''* orbitals of *cis*-butadiene each appear in (**III**) as two components, the second and third h.o.m.o.s (2*a'* and 1*a'*) and second and third l.u.m.o.s (2*a''* and 3*a''*) respectively, each pair of which differ internally in respect of the contributions from boron atoms not in the B(6)B(5)B(10)B(9) face.

A previous[31] EHMO calculation on $\{AuPH_3\}$, that did not include phosphorus 3*d* a.o.s in the basis set, has emphasised the isolobal relationship of this fragment with hydrogen, in that the only fragment orbital in the 'valence band' was the well known gold $6sp_z$ hybrid orbital, since the gold 5*d* a.o.s were considered essentially core orbitals, and the gold $6p_x$, $6p_y$ a.o.s were regarded as too high lying to be effective acceptor orbitals. We have considered the effect of including phosphorus 3*d* a.o.s on the frontier orbitals of $\{AuPH_3\}^+$. Here, the five highest-filled orbitals ($1a_1$ + 1*e* + 2*e*) are, again, essentially (>90%) gold 5*d* in character. The gold $6sp_z$ hybrid orbital ($3a_1$) is slightly stabilised by in-phase combination with phosphorus $3d_{z^2}$, retaining 70% of its gold parentage, and the orbitals of predominantly (*ca.* 80%) gold $6p_x$, $6p_y$ character (5*e*) are somewhat destabilised by out-of-phase mixing with phosphorus $3d_{xz}$, $3d_{yz}$ respectively. Between the h.o.m.o. and the gold $6sp_z$ hybrid come five orbitals that are mainly phosphorus 3*d* in character. However, all of these (which must lie in the 'valence band') have a significant amount of gold character, and the hybridisation at gold, shown in Figure 5(*b*), is such that all are reasonable acceptor orbitals. The 3*e* and 4*e* pairs (both *ca.* 13% gold based) differ in respect of the hybridisation at phosphorus. The $2a_1$ orbital (*ca.* 35% gold in character), which lies slightly lower than the 3*e* pair in a charge-iterated calculation, but slightly higher otherwise, is out of phase between gold and phosphorus, but is lower lying than the (gold-based) $3a_1$ acceptor orbital because of its predominant phosphorus character.

Interaction of (**III**) and (**IV**) in the *z* direction allows net de-occupation of the h.o.m.o. (1*a''*) and second and third h.o.m.o.s (1*a'* and 2*a'*) of (**III**) by virtue of non-zero overlaps with acceptor orbitals on (**IV**) that are *yz*-noded components of *e* pairs and a_1 orbitals respectively, and the relative extents of these interactions determine the formal co-ordination geometry of the gold atom in the product (**V**). Because of the large number of (especially) potential acceptor orbitals of suitable symmetry, we find that interpretation of interfragment overlap integrals is

Table 6. Occupation (electrons) of the first to the third h.o.m.o.s of the fragment (**III**) in (**V**) and in $B_{10}H_{14}$

	h.o.m.o.	2nd h.o.m.o.	3rd h.o.m.o.
In (**V**)			
Including P 3*d* a.o.s			
a	1.665	1.663	1.993
b	1.619	1.743	1.905
Excluding P 3*d* a.o.s			
a	1.848	1.691	1.961
b	1.888	1.791	1.918
In $B_{10}H_{14}$			
a	1.122	1.441	1.763
b	1.124	1.585	1.607

[a] With charge iteration. [b] Without charge iteration.

Table 7. Interfragment overlap integrals

$\{B_{10}H_{12}\}^{2-}$ Donor orbital	$[AuPH_3]^+$ Acceptor orbital	Overlap integral
1*a*″	**6*e*(*x*)**	**0.3033**
	4*e*(*xz*)	0.1251
	3*e*(*xz*)	0.0931
2*a*′	**3a_1**	**0.2822**
	2a_1	0.1964
1*a*′	**3a_1**	**0.1935**
	2a_1	0.1375

* Source: EHMO-FMO calculation without charge iteration. Entries in bold, acceptor orbital predominantly gold-based, entries in normal type, acceptor orbital predominantly phosphorus-based.

largely unhelpful in analysing the bonding in (**V**). However, examination of the occupations of formerly filled fragment m.o.s in (**V**) is more rewarding.

Table 6 lists the occupations of the first three h.o.m.o.s of (**III**) in (**V**) for two methods of calculation (with and without charge iteration) and two basis sets (with and without phosphorus 3*d* a.o.s), as given by EHMO-FMO (FMO = frontier molecular orbital) calculation. Also included for comparison are similar calculations on $B_{10}H_{14}$ fragmented as (**III**) + $\{H\cdots H\}^{2+}$. For the last, deoccupation of the 1*a*′ and 2*a*′ (combined) and 1*a*″ orbitals of (**III**) is essentially equal, consistent with $\{H\cdots H\}^{2+}$ being a zero-electron orbital source. In (**V**), the combined deoccupation of the *a*′ orbitals of (**III**) is, with one exception (phosphorus 3*d* a.o.s included, no charge iteration), always somewhat greater than the deoccupation of the *a*″ h.o.m.o. implying that the $\{AuPH_3\}^+$ fragment is a better radial than tangential acceptor. Whilst this suggests the gold atom is mainly linearly co-ordinated to the B_{10} unit in compound (**2**), the contribution from tangential bonding, which would result in a formally trigonal gold co-ordination geometry were it as strong as the radial component, is clearly not negligible, implying that in (**2**) the metal co-ordination be regarded as intermediate between linear and trigonal. Support for this description derives from the Mössbauer parameters determined for (**2a**) (i.s. 3.68, q.s. 8.13 mm s^{-1}). The fact that the parameters are lower than those for (**1a**) is consistent with the higher connectivity of the gold atom.[17] Although detailed interpretation of these data is limited by a general paucity of Mössbauer studies on gold–boron compounds, it may be significant that the data are again on the low-i.s. edge of the band of values for gold(I) with an orbital number of two, indicating the small involvement of a tangential 6*p* orbital. The lower i.s. value for (**2a**) *versus* (**1a**) is consistent with a higher orbital number for the former.

The data in Table 6 further show that the $\{H\cdots H\}^{2+}$ fragment causes greater deoccupation of the filled orbitals of $\{B_{10}H_{12}\}^{2-}$ than does the $\{AuPH_3\}^+$ fragment. Taken together, the first three h.o.m.o.s of (**III**) are bonding along both the outer [B(5)–B(6), B(9)–B(10)] and inner [B(5)–B(10)] B–B connectivities. Deoccupation of this set of three orbitals will cause both bond types to lengthen, and this nicely explains why, in the structure of (**2a**), (*i*) the average length of the outer connectivity bridged by H [B(6)–B(7), B(8)–B(9) 1.800(21) Å] is appreciably longer than that bridged by gold [B(5)–B(6), B(9)–B(10) 1.721(21) Å], and (*ii*) B(7)–B(8) 2.074(16) Å, is appreciably longer than B(5)–B(10) 1.903(14) Å.

Finally, we note that the EHMO-FMO calculations reveal no perceptible occupation (<0.1 electron) of the l.u.m.o. (3*a*′) of fragment (**III**) in molecule (**V**), *i.e.* no measurable back donation from filled gold $5d_{yz}$ to the cage. Substantial occupation of this fragment orbital in a metal complex would be necessary if the $\{B_{10}H_{12}\}$ ligand were to be regarded as an *arachno* icosahedral fragment carrying a formal 4− charge, so these results are fully consistent with those of both the misfit calculations and the Mössbauer spectrum, *i.e.* in (**2**) the cage is formally the $\{B_{10}H_{12}\}^{2-}$ ligand. The extent of the occupation of the l.u.m.o. of (**III**) is one of the parameters we are monitoring in the thorough analysis of the bonding in $MB_{10}H_{12}$ complexes that we are currently undertaking.[32]

It is particularly significant that the tangential acceptor properties of the gold fragment are emphasised by inclusion of phosphorus 3*d* a.o.s in the basis set, through the 3*e* and 4*e* pairs shown in Figure 5(*b*), and we would argue in favour of the inclusion of phosphorus 3*d* orbitals in future calculations of this sort. However, it is important to note that our support for this wider basis set should not be taken to imply that the (additional) acceptor orbitals of the $\{AuPH_3\}^+$ fragment that are localised on phosphorus are *better* acceptor orbitals than those [3a_1 + 5*e* of Figure 5(*b*)] which are gold-based. Even though the energy matches 6*e*(*x*)/1*a*″ and 3a_1/1*a*′,2*a*′ are clearly worse than 4*e*(*xz*),3*e*(*xz*)/1*a*″ and 2a_1/1*a*′,2*a*′ respectively, the overlap integrals for the former pair are substantially the greater, as documented in Table 7.

The above calculations were performed on a model in which the Au–P vector is perpendicular to the B(6)B(5)B(10)B(9) plane. Tilting the PH_3 unit towards the B(6)B(7)B(8)B(9) plane to mimic more closely the observed geometry of (**2a**) slightly stabilises the molecule, by 0.1—0.2 eV dependent on the calculation. Clearly, the magnitudes of all symmetry-allowed interactions change on tilting, but the greatest effect is seen in the overlap integral between the 2*a*′ orbital of the cage and the $6sp_z$ hybrid of the $\{AuPH_3\}^+$ fragment, which increases from 0.28 to 0.33, and results in an increased occupation of the latter, 0.10 to 0.12 electron. Presumably it is this interaction which drives the distortion, and further emphasises the pseudo-linear nature of the gold atom in (**2**).

Reactions with Acids.—The deprotonation-induced slipping of μ-$AuPR_3$ in compound (**1**) to μ_4-$AuPR_3$ in (**2**) appears to be fully reversible, since reaction of the $[NHEt_3]^+$ salt of (**2a**) with a molar equivalent of CF_3CO_2H immediately affords (**1a**) as the only phosphorus-containing species. EHMO calculations confirm that the h.o.m.o. of (**V**) is antibonding between gold and the B(6)–B(5) and B(9)–B(10) edges. Furthermore, in CH_2Cl_2, the (remaining) BAuB three-centre bond of (**1a**) is cleaved by HCl, producing $[AuCl\{P(C_6H_{11})_3\}]$ and $B_{10}H_{14}$, identified by ^{31}P-$\{^1H\}$ and ^{11}B-$\{^1H\}$ n.m.r. spectroscopies respectively. We have already[1] shown that $[AuCl\{P(C_6H_{11})_3\}]$ reacts with $B_{10}H_{13}^-$ to afford complex (**1a**).

By these studies we have demonstrated the stepwise and reversible attainment of η^2 and η^4 ligation of a metal fragment by a B_{10} cage, going from $B_{10}H_{14} \longleftrightarrow \eta^2\text{-}\{B_{10}H_{13}\}^- \longleftrightarrow \eta^4\text{-}\{B_{10}H_{12}\}^{2-}$. This work may shed mechanistic light on the observation [33] that species like $[Zn(OEt_2)_n(\eta^4\text{-}B_{10}H_{12})]$ are cleaved by HCl to produce $B_{10}H_{14}$, and serve as model studies for cleavage of the B_{10} units from the triple cluster compounds [29] $[(B_{10}H_{12}Au)(AuPR_3)_4(AuB_{10}H_{12})]$ (R = Et or Ph) as a novel route to gold cluster compounds. We will report the results of these reactions in a future contribution to this series.

Acknowledgements

We thank the International Gold Corporation and Johnson Matthey for generous loans of gold salts, and Dr. D. Reed for $^1H\text{-}\{^{11}B\}$ and $^{11}B\text{-}\{^1H\}$ n.m.r. spectra and helpful discussions.

References

1 Part 1, A. J. Wynd, A. J. McLennan, D. Reed, and A. J. Welch, *J. Chem. Soc., Dalton Trans.*, 1987, 2761.
2 G. B. Jacobsen, D. G. Meina, J. H. Morris, C. Thomson, S. J. Andrews, A. J. Welch, and D. F. Gaines, *J. Chem. Soc., Dalton Trans.*, 1985, 1645.
3 A. J. Wynd, Ph.D. Thesis, University of Edinburgh, 1988; A. J. Wynd and A. J. Welch, unpublished work.
4 N. G. Walker and D. Stuart, DIFABS, *Acta Crystallogr., Sect. A*, 1983, **39**, 158.
5 R. O. Gould and P. Taylor, CALC, University of Edinburgh, 1986.
6 'International Tables for *X*-Ray Crystallography,' Kynoch Press, Birmingham, 1974, vol. 4, p. 99.
7 G. M. Sheldrick, SHELX 76, University of Cambridge, 1976.
8 R. O. Gould and D. E. Smith, CADABS, University of Edinburgh, 1986.
9 P. Mallinson, EASYORTEP, University of Glasgow, 1982.
10 J. Howell, A. Rossi, D. Wallace, K. Haraki, and R. Hoffmann, ICON8, Quantum Chemistry Program Exchange, University of Indiana, 1977, no. 344.
11 J. H. Ammeter, H-B. Burgi, J. C. Thibeault, and R. Hoffmann, *J. Am. Chem. Soc.*, 1982, **100**, 3686.
12 R. Brill, H. Dietrich, and H. Dierks, *Acta Crystallogr., Sect. B*, 1971, **27**, 2003.
13 D. C. Finster and R. N. Grimes, *Inorg. Chem.*, 1981, **20**, 863.
14 G. F. Mitchell and A. J. Welch, *J. Chem. Soc., Dalton Trans.*, 1987, 1017.
15 R. V. Parish in 'Mössbauer Spectroscopy Applied to Inorganic Chemistry,' ed. G. J. Long, Plenum, New York, 1984, vol. 1, p. 577; *Gold Bull.*, 1982, **15**, 51; *Chem. Brit.*, 1985, **21**, 740.
16 R. V. Parish, L. S. Moore, A. J. J. Dens, D. M. P. Mingos, and D. J. Sherman, *J. Chem. Soc., Dalton Trans.*, 1989, 539.
17 R. V. Parish, *Hyperfine Interact.*, 1988, **40**, 159.
18 R. Uson, A. Laguna, A. Navarro, R. V. Parish, and L. S. Moore, *Inorg. Chim. Acta*, 1986, **112**, 205.
19 G. C. H. Jones, P. G. Jones, A. G. Maddock, M. J. Mays, P. A. Vergnano, and A. F. Williams, *J. Chem. Soc., Dalton Trans.*, 1977, 1440.
20 K. Wade, *Adv. Inorg. Chem. Radiochem.*, 1976, **18**, 1.
21 See, for example, D. M. P. Mingos, M. I. Forsyth, and A. J. Welch, *J. Chem. Soc., Dalton Trans.*, 1978, 1363,
22 J. D. Kennedy, *Prog. Inorg. Chem.*, 1986, **34**, 326.
23 J. D. Kennedy, *Prog. Inorg. Chem.*, 1986, **34**, 343.
24 D. S. Kendall and W. N. Lipscomb, *Inorg. Chem.*, 1973, **12**, 546.
25 C. J. Fritchie, *Inorg. Chem.*, 1967, **6**, 1199.
26 L. G. Sneddon, J. C. Huffman, R. O. Schaeffer, and W. E. Streib, *J. Chem. Soc., Chem. Commun.*, 1972, 474.
27 A. J. Wynd and A. J. Welch, *Acta Crystallogr., Sect. C*, 1989, **45**, 615.
28 A. J. Wynd and A. J. Welch, *J. Chem. Soc., Chem. Commun.*, 1987, 1174.
29 A. J. Wynd, S. E. Robins, D. A. Welch, and A. J. Welch, *J. Chem. Soc., Chem. Commun.*, 1985, 819.
30 W. L. Jørgenson and L. Salem, 'The Organic Chemist's Book of Orbitals,' Academic Press, New York, 1973.
31 D. G. Evans and D. M. P. Mingos, *J. Organomet. Chem.*, 1982, **232**, 171.
32 A. J. Wynd, S. A. Macgregor, L. J. Yellowlees, and A. J. Welch, unpublished work.
33 N. N. Greenwood and N. F. Travers, *J. Chem. Soc. A*, 1968, 15.

Received 8*th December* 1988, *revised manuscript received* 23*rd November* 1989; *Paper* 8/04852E